Electronic Supplementary Material (ESI) for Lab on a Chip.

Supplementary Information

Single cell migration profiling on a microenvironmentally tunable hydrogel microstructure device enable stem cell potency evaluation.

Enrique Ros,[a,b] Matías Encina,[a,b] Fabian Gonzalez,[a,b] Rafael Contreras,[c] Patricia Luz-Crawford,[c] Maroun Khoury,[a,b,d] and Juan Pablo Acevedo[a,b,d]*

a. Cells for Cells, Santiago, Chile.

b. Consorcio Regenero, Chilean Consortium for Regenerative Medicine, Santiago, Chile.

c. Laboratorio de Inmunología Celular y Molecular, Centro de Investigación Biomédica, Facultad de Medicina, Universidad de los Andes, Santiago, Chile.

d. Laboratory of Nano-Regenerative Medicine, Faculty of Medicine, Universidad de los Andes, Santiago, Chile. E-mail: jpacevedo@uandes.cl

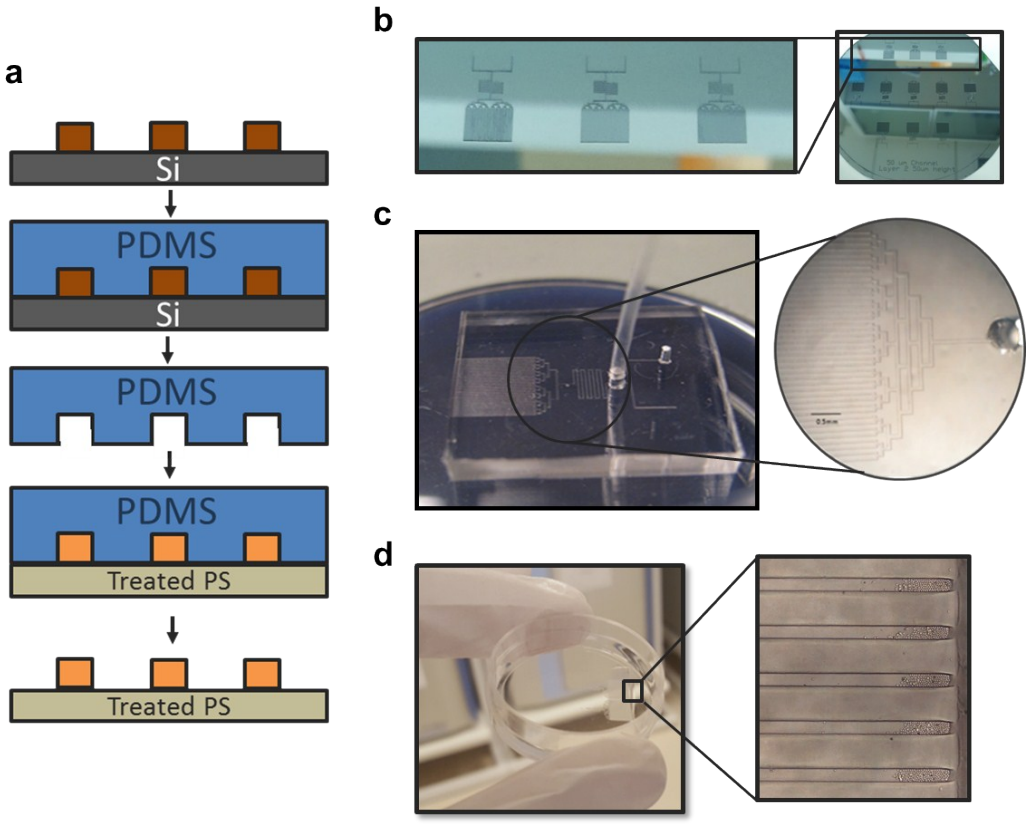

Figure S1. Device microfabrication. a) Schematic fabrication of the migration device. Fabrication starts with a primary mold mounted on a silicon wafer (Si) harbouring connected and parallel lines of SU-8 photoresistant material (brown features). Afterward, soft lithography was used to obtain a polydimethylsiloxane (PDMS) secondary mold. Finally, the PDMS mold is bonded to the bottom surface of the polystyrene culture Petri dish (Treated PS) and microinjected with a GelMA solution using a syringe microfluidic pump. Microinjected PDMS molds are afterward UV irradiated to induce GelMA-based hydrogel formation and peeled off to obtain the stamped migration lanes on the bottom Surface of the Petri dish. b) Example of primary silicon/SU-8 mold. c) Example of PDMS secondary mold during microinjection of GelMA solution. d) Example of the hydrogel walls physically limiting the migration lanes.

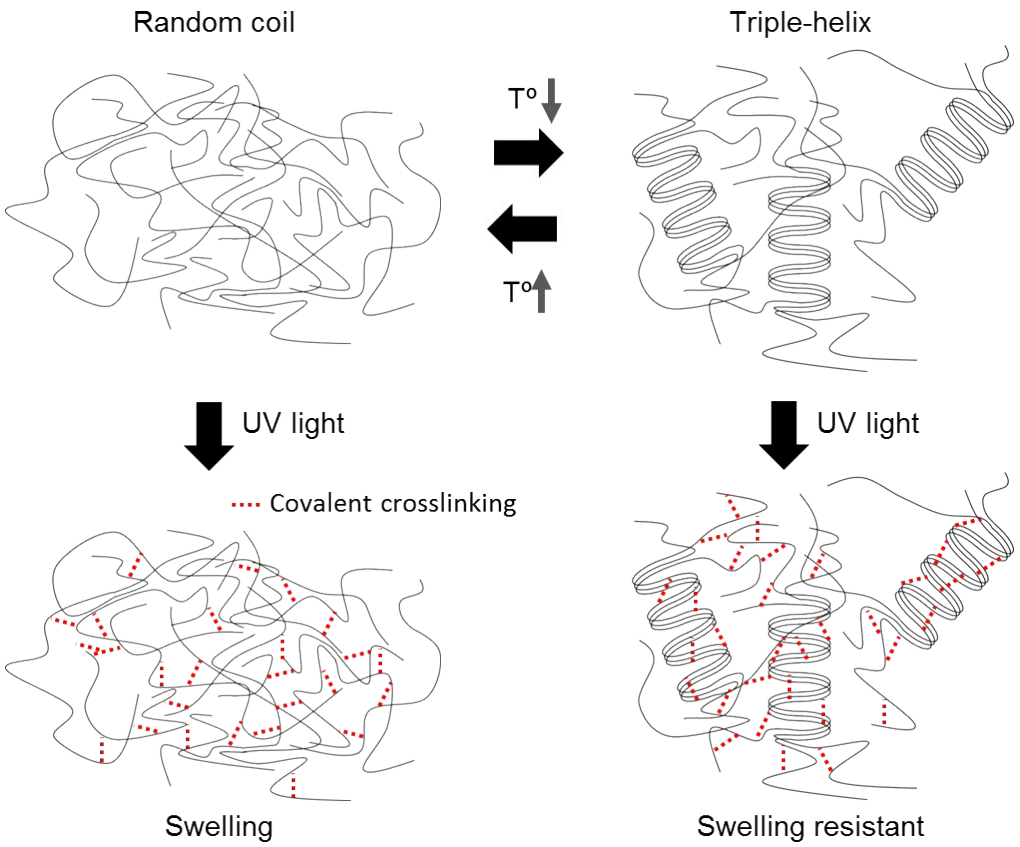

Figure S2. Schematic representation of polymeric conformation of gelatin methacrylamide (GelMA) in solution under thermal and UV induction. At higher temperature, gelatin is conformed as random coil in solution, whereas at lower temperatures triple-helix formation is induced during the process of gelation or physical crosslinking. GelMA solution in presence of photoinitiators and UV induction undergo covalent crosslinking, however, if such photo-crosslinking is conducted under random coil configuration, hydrogels in PBS 1X pH 7.4 suffer of swelling and volumetric increment. On the other hand, if UV induction is performed under triple-helix conformation (gelated), hydrogel swelling is avoided.

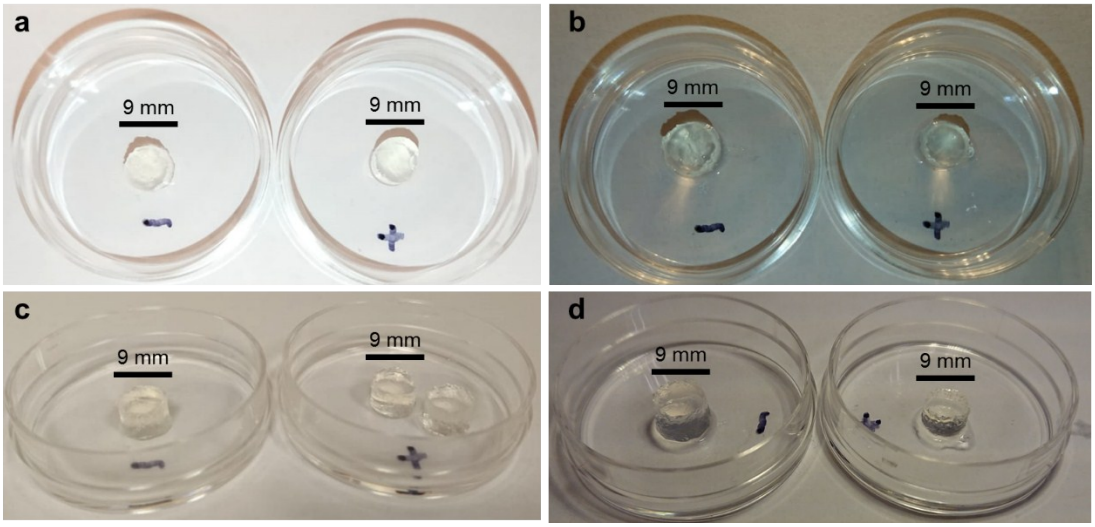

Figure S3. Visual example of the non-swelling and swelling effect over photo-crosslinked hydrogel with and without previous induction of thermal physical crosslinking (gelation) respectively. Top view (a) and lateral view (c) of a recently photo-crosslinked GelMA hydrogel without (left) and with (right) previous physical crosslinking or gelation. Top view (b) and lateral view (d) of a photo-crosslinked GelMA hydrogel without (left) and with (right) previous physical crosslinking or gelation. Hydrogels imaged in (b) and (d) were incubated in PBS 1X pH 7.4 for 12 h at room temperature.

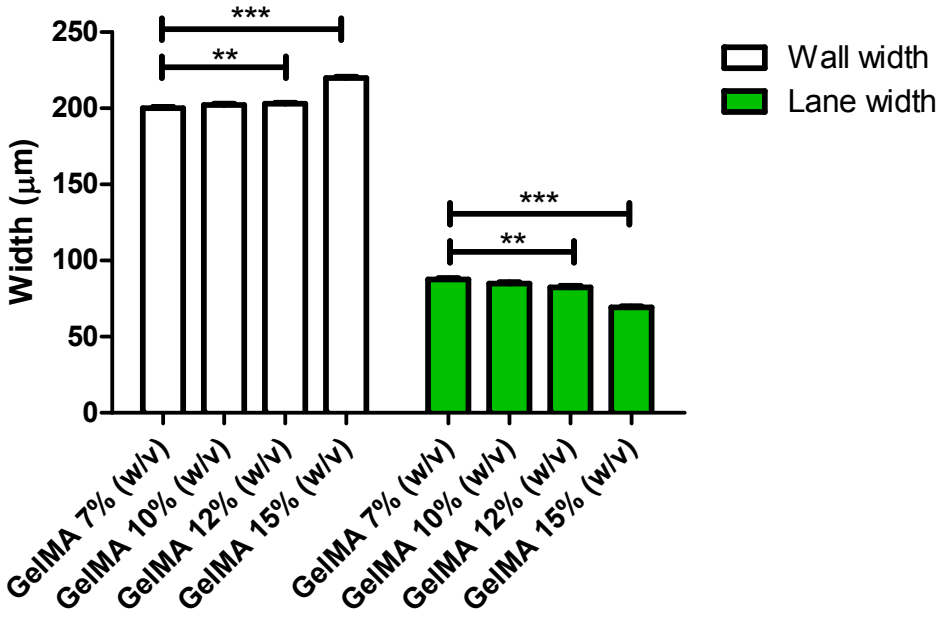

Figure S4. Dimensional variations of hydrogel walls and migration lanes in the new migration device submitted to swelling. Hydrogel walls were fabricated using different concentrations of GelMA solution, and after fabrication through microinjection of the PDMS mold, physical cross-linking (2h at 4°C), UV-irradiation and PDMS mold removal performed. They were subjected to incubation for 3 h in PBS 1X pH 7.4 at 37ºC. Width of hydrogel walls and migration lane were quantified using light microscopy and statistically compared between the GelMA 7% (v/w) formulation and all the other formulations. Three devices per formulation were analyzed and 12 hydrogel and lane measurements conducted per each device. Error bars

= standard error of the mean. ** p<0.01; *** p<0.001. Statistical analysis was conducted using the Mann–Whitney U test.

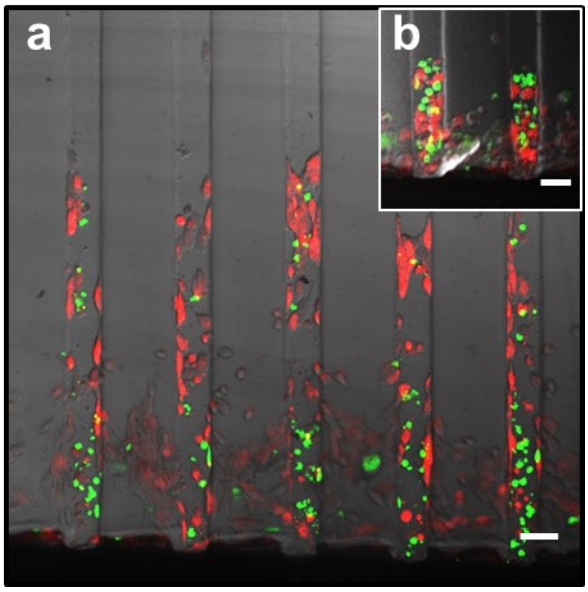

Figure S5. Migration assay using the new migration device and the co-culturing of two different UC-MSCs samples. UC-MSCs samples were stained separately with different fluorescent membrane dyes and co-cultured in the migration device in a 1:1 ratio. The two population have different migration capacity, slow migrating population (green) and fast migrating population (red). After the migration assay these populations are separated along the migration lanes. Scale bar: 50 µm.

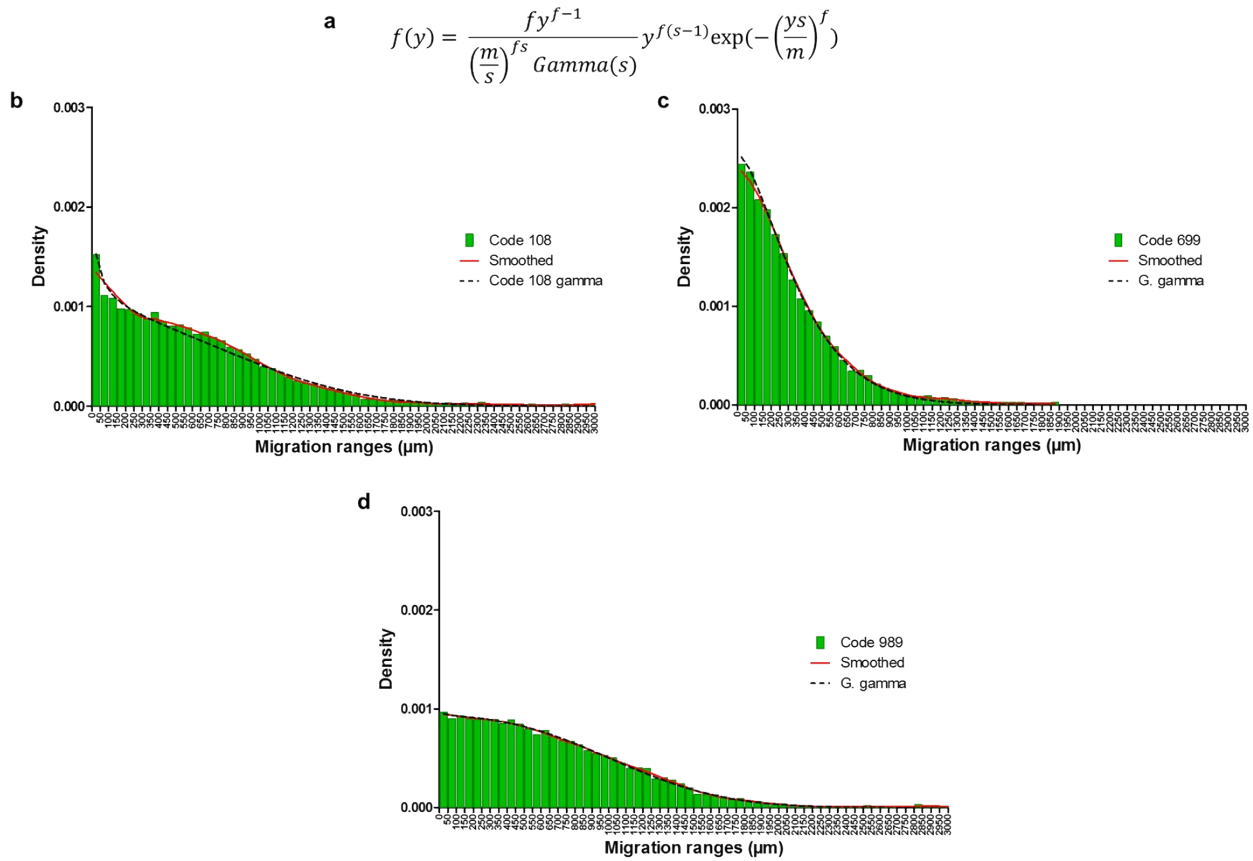

Figure S6. Distribution of migrated distances of three different UC-MSCs populations represented as density distribution. a) multi-parametric generalized gamma distribution as density function *f(y),* where *m* is the scale parameter, *s* is the shape and *f* is the family parameter of the distribution. This function can be used to describe the density distribution of migrated distances of cells in a cell population after maximum-likelihood fitting process to find appropriated parameters values. b) Density distribution of code 108 of a UC-MCS population represented as histogram (green bars), as a connected line derived from a 2nd order of smoothing polynomial using 6 neighbors data to average (red line) and as a multiparametric generalized gamma density function (dashed black line). The same processing was applied to code 699 (c) and code 989 (d). It is important to notice that the generalized gamma function is capable to represent the migration distribution with appropriated fidelity in the three different forms of migration distribution. Density of migrated cells at each migration range of 50 µm (green bars) was calculated from the migration result of 6 migration devices.

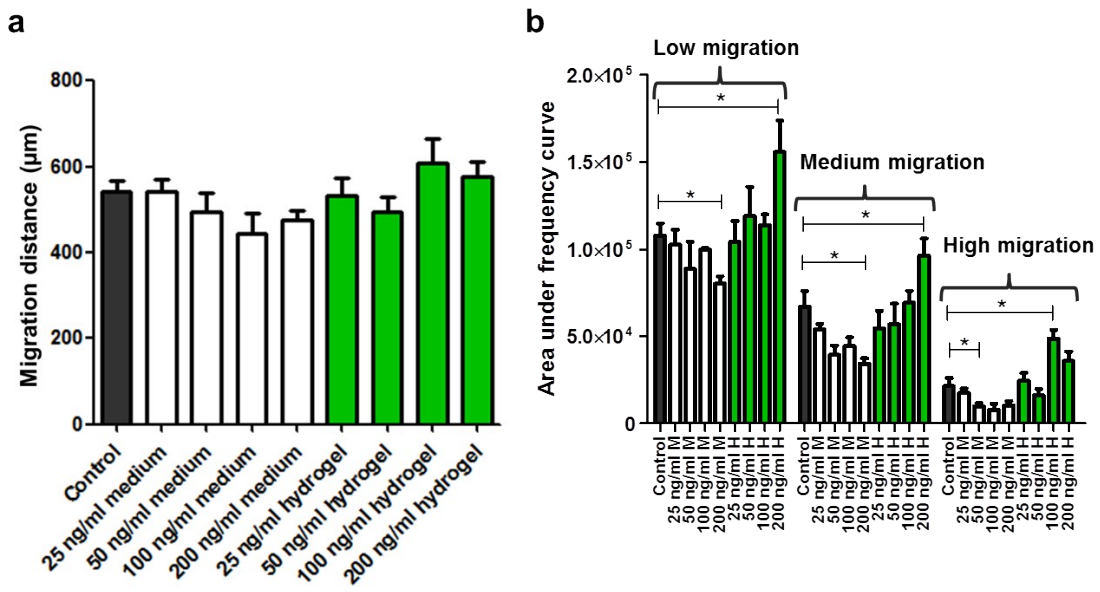

Figure S7. Migration results and distribution of migrated cells of a UC-MSCs population using encapsulated VEGF or soluble VEGF in the media using the new migration device. a) Average migration distance of cells that migrated out from the cell packing zone in response to different concentrations of VEGF presented in the media or encapsulated in the hydrogel walls. d) Area under the curve of frequency distribution (Fig. 3d in the main manuscript) for subpopulations of low, medium and high migration, where low migration quantifies the area under the curve from 0 to 500 µm, medium migration from 500 to 1000 µm and high migration from 1000 µm to the location of the most distanced cell. Control = no treatment or 0 ng/ml of VEGF. Statistical analysis was conducted using two tailed Mann–Whitney U test, 95% of confidence was used and significance was denoted as *p ≤ 0.05. Results are presented as mean ± SEM. n = 4 independent experiments.

Consideration respect to the number of seeded cells

Cell density has been considered an important factor that influences cell migration behaviour (1–5), therefore, it has to be treated carefully for experimental settings and designs, especially in Boyden chamber and scratch assays(6). In this work, the effect of the number of seeded cells on the migration results has been evaluated using this device with umbilical cord mesenchymal stem cells (UC-MSCs). The percentage of migrating cells from the total number of seeded cells and average migrated distances were calculated for devices seeded with different number of cells from the same cell sample. Results showed slight tendencies toward a reduction in the percentage of migrated cells at a higher number of seeded cells (Fig. S8a), whereas for the average migration distance there are incrementally higher values at higher number of seeded cells (Fig. S8b). This is as well corroborated if the relative frequency distribution of cell distances are plotted and compared (Fig. S8c and S8d). The reduced percentage of migrated cells at higher number of seeded cells could be simply explained by steric hinderance, where cells are obstructed by other cells to freely migrate along migration lanes. On the other hand, devices using lower ranges of seeded cells show reduction in the migration distance (average), possible due to the inability of few separated cells to generate

the cell-cell interaction and inter-cellular signalling necessary for performing efficient collective or semi-collective cell migration (4,5). These results demonstrate, in general terms, the robustness against variations in the number of seeded cells, however, it must be considered that too much reduction or increase in the number of seeded cells could slightly affect the migration distribution.

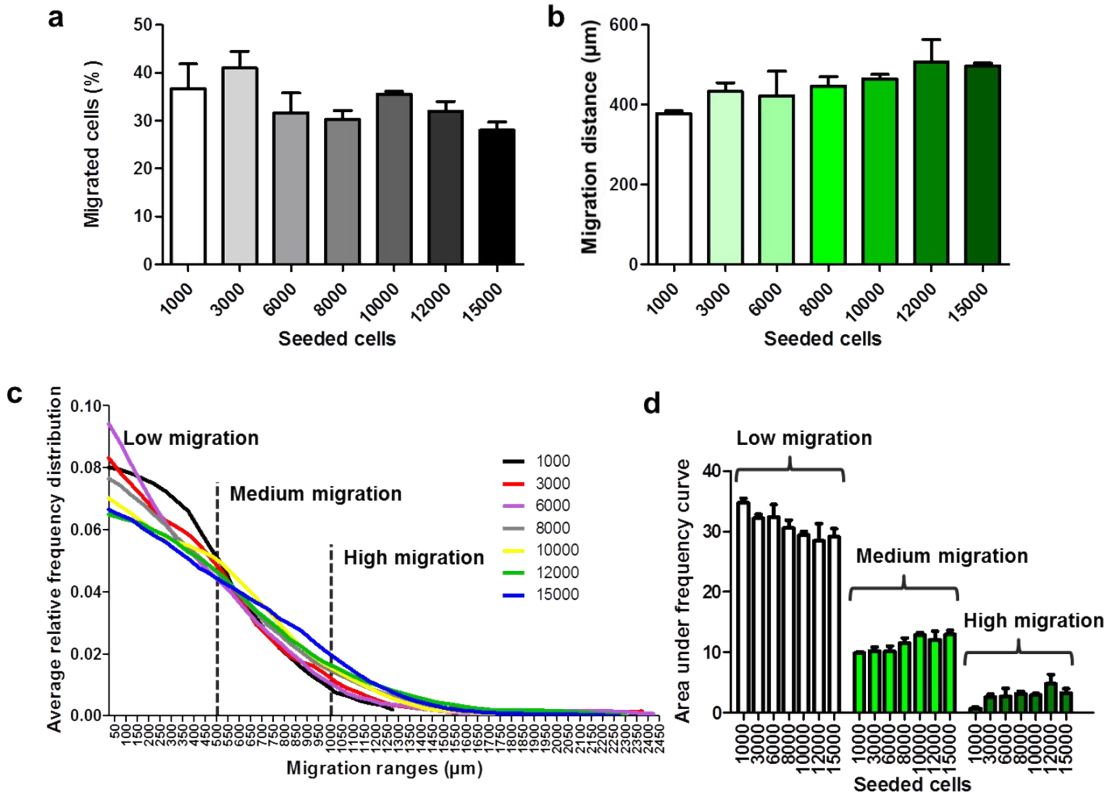

Figure S8. Migration results and distribution of migrated cells of a UC-MSCs population using different number of seeded cells in the new migration device. a) Percentage of cells from the total number of seeded cells that migrated out from the cell packing zone. b) Average migration distance of cells that migrated out from the cell packing zone. c) Average relative frequency distribution of migrated cells at different ranges of migration. Every point of frequency calculation corresponds to the relative number of cells within 50 µm range along the migration lane. The relative frequency is calculated considering the total number of migrated cells. d) Area under the curve of frequency distribution for subpopulations of low, medium and high migration, where low migration quantifies the area under the curve from 0 to 500 µm, medium migration from 500 to 1000 µm and high migration from 1000 µm to the location of the most distanced cell. Results are presented as mean ± SEM. n = 6 independent experiments.

Consideration respect to the width of migration lanes

Cell migration velocity within confined channels has been previously reported of having both, negative correlation (7) or positive correlation (8) with respect to the migrational channel width. Negative correlation has been observed when confinement is defined by the width of cell attachment surfaces for migration, without spatial restriction to the rest of the cellular body, while positive correlation is observed when confinement involved physical restriction to the cellular body, going from 3 μm to 50 μm. In this particular study, evaluations concerning the effect of lane width on cell migration response were conducted using two cell types with different average diameter, human umbilical vessel endothelial cells (HUVEC) (~ 15 μm) and UC-MSCs (~30 μm) (Fig. S9) (9,10), however, it is important to make notice that physical confinement is subjected only at the width level in the new device, and not at the height, since migration lanes are open or roofless. Another distinctive feature of this device is that the 3D wall-bottom surfaces interception creates a groove-like topography in which cells are prompted to confine, resembling a 3D environment. In this regards, and as described previously (11-17), actin polymerization perpendicular to the intercepting surfaces line or groove line would generate compressive forces over growing actin networks from non-contacting cell membranes, that drives uniaxial protrusion in the direction of migration lanes (16). As anticipated for migration lanes with two lateral wall-bottom interceptions, exceedingly narrow migration lanes results in physical impedance for cell body movements along two rows of migrating cells too close to each other, thus only one row of migrating cells is permitted; resulting in less number of migrated cells (Fig. S9). Surprisingly, although broader migration lanes provide two lateral migration clefts, overly broad lanes resulted in a reduction in the number of migrated cells and in the migrated distances. In this case the limitation is related to the time that cells require finding a free spot at the wall-bottom surface interception to drive after migration along the cleft track.

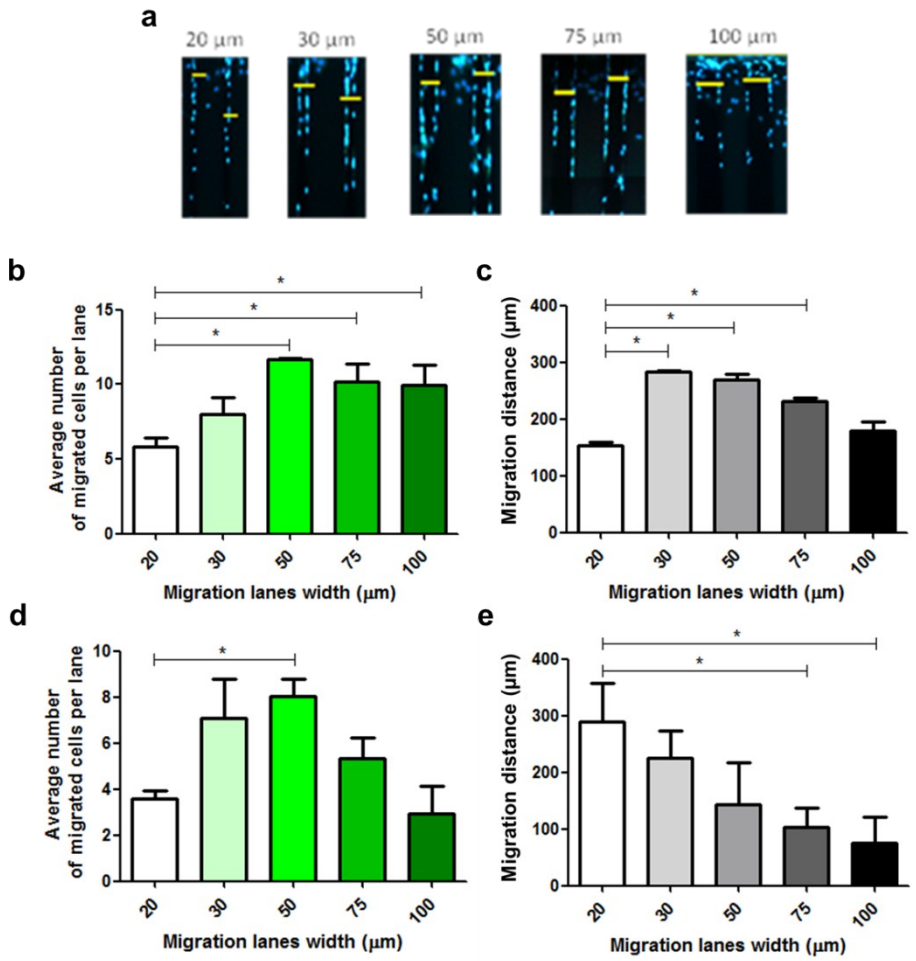

Figure S9. Migration response of HUVECs and UC-MSCs using migration lanes with different width. a) Representative figures of nucleus stained HUVECs migrated along migration lanes with different widths. Yellow lines represent location of the cell packing zone on time 0 b) Average number of migrated HUVECs per migration lane. c) Average migration distance of migrated HUVECs using migration lanes with different widths. d) Average number of migrated UC-MSCs per migration lane. c) Average migration distance of migrated UC-MSCs using migration lanes with different widths. Statistical analysis was conducted using two tailed Mann–Whitney U test, 95% confidence was used and significance was denoted as *$p \leq 0.05$. Results are presented as mean ± SEM. n = 4 independent experiments.

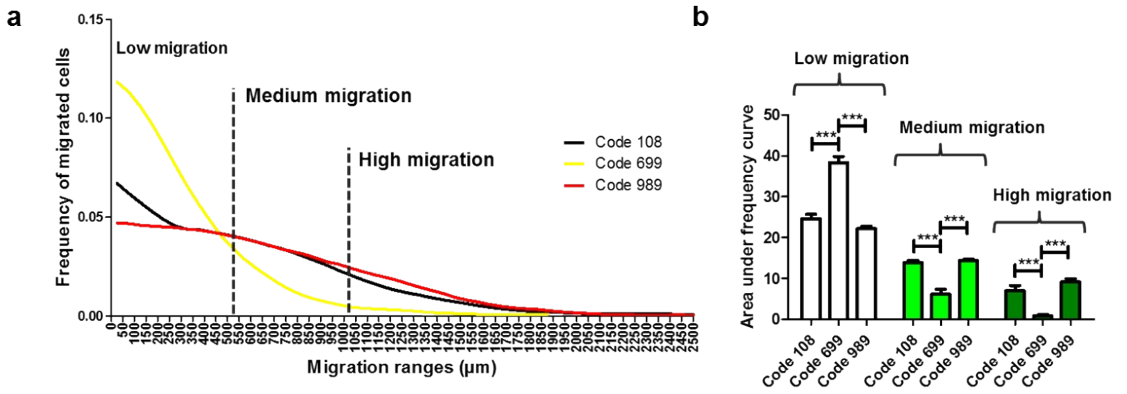

Figure S10. Comparative migration study of different UC-MSCs donor codes using the new migration device. a) Relative frequency of migrated cells of three different donor codes along the migration lanes. f) Area under the frequency curve of three different donor codes for subpopulations of low migration response (migration from 0 to 500 µm), medium migration (from 500 to 1000 µm) and high migration (from 1000 µm to the location of the more distanced cell). All migration assays using the new migration device were performed in presence of 3% FBS in the incubation media for 18 h. Statistical analysis was conducted using two tailed Mann–Whitney U test, 95% of confidence was used and significance was denoted as *p ≤ 0.05, **p ≤ 0.01 and ***p ≤ 0.005. Results are presented as mean ± SEM. n = 12 independent experiments.

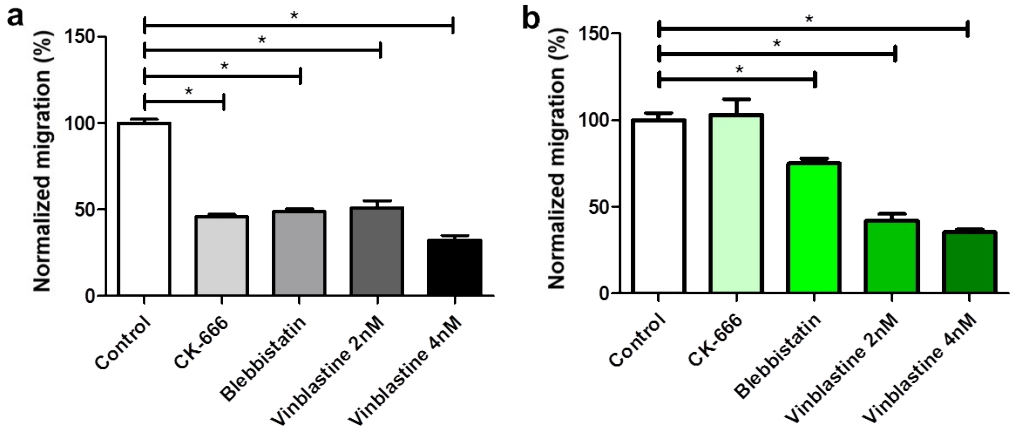

Figure S11. Migration results using the Boyden chamber (a) and the new device (b) in presence of different migration inhibitors. a) Migration results of UC-MSCs code 108 using the Boyden chamber in presence of different inhibitors. The assay was carried out using an incubation media supplemented with 0.1% of FBS in the upper chamber and 3% FBS in the bottom chamber. Quantification was done calculating the percentage of cell-covered area in the bottom face of the porous membrane after 18 h of incubation. b) Average migration distance of cells in a cell sample of UC-MSCs code 108 using the new migration device in presence of different migration inhibitors. The assay was carried out using an incubation media supplemented with 3% of FBS and for 18 h. Min-max normalization procedure was applied to allow comparisons in between different migration systems. CK-666 and Blebbistatin were supplemented at a concentration of 50 µM. Control = without presence of inhibitors. Statistical analysis was conducted using two tailed Mann–Whitney U test, 95% confidence was used and significance was denoted as *p ≤ 0.05. Results are presented as mean ± SEM. n = 9 independent experiments.

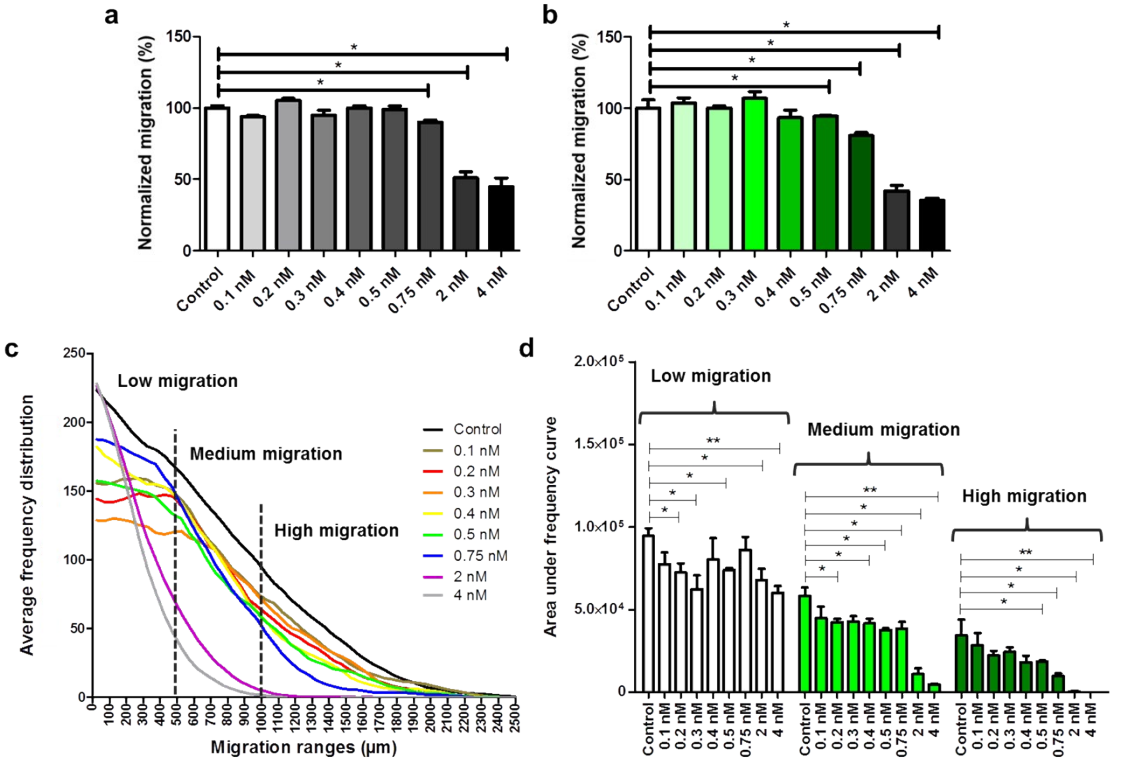

Figure S12. Migration results and distribution of migrated cells of a UC-MSCs population (code 108) subjected to different concentrations of the migration inhibitor Vinblastine. a) Boyden chamber assay using UC-MSCs sample (donor code 108) in the presence of different concentration of the inhibitor Vinblastine. Assay was carried out using an incubation media supplemented with 0.1% of FBS in the upper chamber and 3% FBS in the bottom chamber. Quantification was performed calculating the percentage of cell-covered area in the bottom face of the porous membrane after 18 h of incubation. b) Quantification of migration response using the new migration device and based on the average migrated distance of migrated cells out from the cell packing zone. c) Average frequency of migrated cells along the migration lanes in presence of different concentration of Vinblastine. f) Area under the frequency curve of migrated cells along the migration lane, individualizing the subpopulations of low migration response (cells showing migration from 0 to 500 µm), medium migration (from 500 to 1000 µm) and high migration (from 1000 µm to the location of the most distanced cell). All migration assays using the new migration device were performed in presence of 3% FBS in the incubation media for 18 h. Min-max normalization procedure was applied to allow comparisons in between different migration systems. Control = no treatment or 0 nM concentration of Vinblastine. Statistical analysis was conducted using two tailed Mann–Whitney U test, 95% of confidence was used and significance was denoted as *$p \leq 0.05$ and **$p \leq 0.01$. Results are presented as mean ± SEM. n = 6 independent experiments.

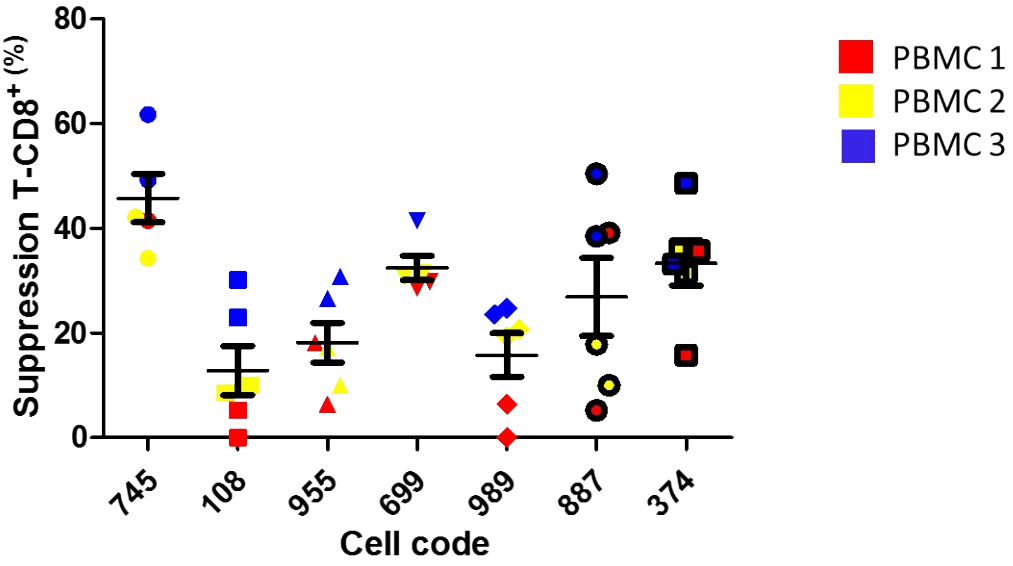

Figure S13. Immunosupression of T-CD8⁺ in 3 different peripheral blood mononuclear cell samples (PBMCs) treated with PHA for proliferation activation in presence of UC-MSCs from different donor codes. The UC-MSCs:PBMCs ration during proliferation incubation was 1:50. Results are presented as mean ± SEM. n = 3 biological replicates (PBMCs) with 2 experimental replicates.

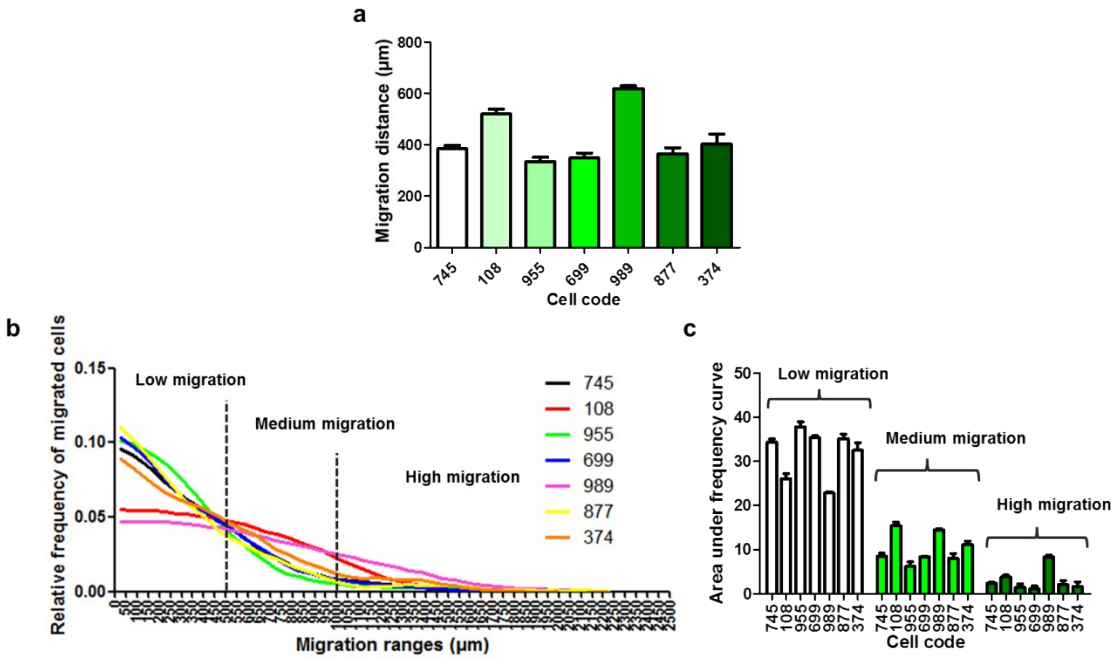

Figure S14. Migration results and distribution of migrated cells of UC-MSCs samples from different donor codes. a) Average migration of cells that migrated out from the cell packing zone. b) Average relative frequency distribution of migrated cells at different ranges of migration. Every point of frequency calculation corresponds to the relative number of cells within 50 µm range along the migration lane. c) Area under the curve of frequency distribution for subpopulations of low, medium and high migration, where low migration quantifies the

area under the curve from 0 to 500 µm, medium migration from 500 to 1000 µm and high migration from 1000 µm to the location of the most distanced cell. Results are presented as mean ± SEM. n = 6 independent experiments.

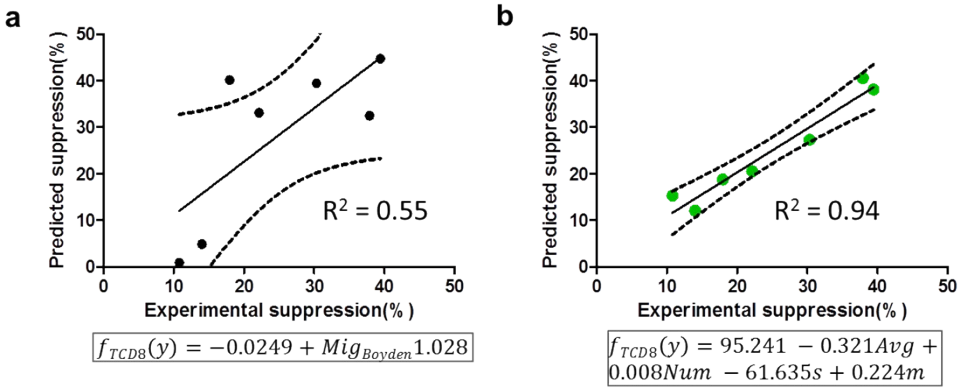

Figure S15. Correlation of predicted immunosuppressive values and experimental immunosuppression values. a) Predicted immunosuppression values were extracted based on a linear regression (framed model) constructed using migration responses in the Boyden chamber system and experimental immunosuppressive values of different UC-MSC code donors. b) Predicted immunosuppression values were extracted based on a multiparametric elastic-net regression (framed model) constructed using 5 different parameters obtained from the migration responses in the new migration device and experimental immunosuppressive values of different UC-MSC code donors. Immunosuppression was calculated based on the proliferative suppression of $CD8^+$ cells.

Table S1. Quantified parameters of the generalized gamma distribution describing the probability distribution of migrated distances (s, m and f as defined in the function “dggamma” implemented in the package “rmutil” in the software R) of different UC-MSCs sample codes. Additionally, average migration distance of migrated cells and number of migrated distances for each cell code. Percentage of proliferation suppression of 3 activated PBMC sample in presence of different UC-MSC donor codes.

Code	s	m	f	Average (µm)	Number of Cells	Suppression T-Cell CD8+ (%)
745	0.76	389.84	1.40	384.46	2793.33	39.43
108	0.33	331.13	3.17	520.00	3616.25	10.80
955	0.96	307.67	1.42	333.38	2246.00	17.96
699	0.47	297.91	2.06	348.00	2028.67	37.91
989	0.28	357.36	3.53	618.84	5945.67	14.00
877	0.66	338.45	1.63	365.12	540.75	22.16
374	0.28	249.64	3.21	402.93	2435.25	30.35

References supplementary information

1. Wong IY, Javaid S, Wong EA, Perk S, Haber DA, Toner M, et al. Collective and individual migration following the epithelial–mesenchymal transition. *Nature Materials*. [Online] Nature Publishing Group; 2014;13(11): 1063–1071.
2. Jin W, Shah ET, Penington CJ, McCue SW, Chopin LK, Simpson MJ. Reproducibility of scratch assays is affected by the initial degree of confluence: Experiments, modelling and model selection. *Journal of Theoretical Biology*. [Online] 2016;390: 136–145.
3. Rosen P, Misfeldt DS. Cell density determines epithelial migration in culture. *Proceedings of the National Academy of Sciences of the United States of America*. [Online] 1980;77(8): 4760–4763.
4. Mayor R, Etienne-Manneville S. The front and rear of collective cell migration. *Nature Reviews Molecular Cell Biology*. [Online] Nature Research; 2016;17(2): 97–109.
5. Scarpa E, Mayor R. Collective cell migration in development. *The Journal of Cell Biology*. [Online] 2016;212(2): 143–155.
6. Liang C-C, Park AY, Guan J-L. In vitro scratch assay: a convenient and inexpensive method for analysis of cell migration in vitro. *Nature Protocols*. [Online] Nature Publishing Group; 2007;2(2): 329–333.
7. Vedula SRK, Leong MC, Lai TL, Hersen P, Kabla AJ, Lim CT, et al. Emerging modes of collective cell migration induced by geometrical constraints. *Proceedings of the National Academy of Sciences of the United States of America*. [Online] National Academy of Sciences; 2012;109(32): 12974–12979.
8. Tong Z, Balzer EM, Dallas MR, Hung W-C, Stebe KJ, Konstantopoulos K. Chemotaxis of Cell Populations through Confined Spaces at Single-Cell Resolution. Rao C V. (ed.) *PLoS ONE*. [Online] 2012;7(1): e29211.
9. Prickett RC, Marquez-Curtis LA, Elliott JAW, McGann LE. Effect of supercooling and cell volume on intracellular ice formation. *Cryobiology*. [Online] Academic Press; 2015;70(2): 156–163.
10. Chen G, Yang T, Qiao M, Liu H, Depei W. Comparative Study of the Biological Characteristics of Serum-Free and Fetal Bovine Serum-Contained Medium Cultured Umbilical Cord-Derived Mesenchymal Stem Cells. *Blood*. [Online] American Society of Hematology; 2012;120(21): 4737–4737.
11. Doyle AD, Wang FW, Matsumoto K, Yamada KM. One-dimensional topography underlies three-dimensional fibrillar cell migration. *The Journal of cell biology*. [Online] 2009;184(4): 481–490.
12. Wilson K, Lewalle A, Fritzsche M, Thorogate R, Duke T, Charras G. Mechanisms of leading edge protrusion in interstitial migration. Nature Communications. [Online] 2013;4(1): 2896.
13. Kim LY, Thompson PM, Lee HT, Pershad M, Campbell SL, Alushin GM. The Structural Basis of Actin Organization by Vinculin and Metavinculin. Journal of Molecular Biology. [Online] Academic Press; 2016;428(1): 10–25.
14. Thievessen I, Fakhri N, Steinwachs J, Kraus V, McIsaac RS, Gao L, et al. Vinculin is required for cell polarization, migration, and extracellular matrix remodeling in 3D collagen. FASEB journal : official publication of the Federation of American Societies for Experimental Biology. [Online] The Federation of American Societies for Experimental Biology; 2015;29(11): 4555–4567.
15. Hawkins RJ, Piel M, Faure-Andre G, Lennon-Dumenil AM, Joanny JF, Prost J, et al. Pushing off the Walls: A Mechanism of Cell Motility in Confinement. Physical Review Letters. [Online] 2009;102(5): 58103.
16. Kushiro K, Sakai T, Takai M. Slope-Dependent Cell Motility Enhancements at the Walls of PEG-Hydrogel Microgroove Structures. Langmuir. [Online] American Chemical Society; 2015;31(37): 10215–10222.
17. Kushiro K, Yaginuma T, Ryo A, Takai M. Differences in Three-Dimensional Geometric Recognition by Non-Cancerous and Cancerous Epithelial Cells on Microgroove-Based Topography. Scientific Reports. [Online] Nature Publishing Group; 2017;7(1): 4244.